Korean J. Chem. Eng., 40(6), 1440-1456 (2023)
DOI: 10.1007/s11814-023-1434-y

pISSN: 0256-1115
eISSN: 1975-7220

Adsorption kinetics, equilibrium, and thermodynamic studies to understand adsorption behavior of Evans blue dye by durian husk

Ain Aqilah Basirun*, Ahmad Razi Othman, Nur Adeela Yasid*, Mohd Izuan Effendi Halmi***, Baskaran Gunasekaran****, and Mohd Yunus Abd Shukor*,†**

*Department of Biochemistry, Faculty of Biotechnology and Biomolecular Science Universiti Putra Malaysia, 43400 UPM Serdang, Selangor, D.E, Malaysia
**Department of Chemical and Process Engineering, Faculty of Engineering and Built Environment, Universiti Kebangsaan Malaysia, 43600 UKM Bangi, Selangor, D.E, Malaysia
***Department of Soil Management, Faculty of Agriculture Universiti Putra Malaysia, 43400 UPM Serdang, Selangor, D.E, Malaysia
****Faculty of Applied Science, UCSI University, UCSI Heights, 1, Jalan Puncak Menara Gading, Taman Connaught, 56000 Cheras, Wilayah Persekutuan Kuala Lumpur, Malaysia
(*Received 18 June 2022 • Revised 3 December 2022 • Accepted 31 January 2023*)

Abstract−Membrane isolation, ion exchange, precipitation, transformation, and biosorption are all viable methods for pollutant removal. Adsorption is a common commercial method to concentrate precious molecules or eliminate contaminants, and it is a cost-effective method of treating industrial wastewater. A novel method for increasing their removal effectiveness has been developed for this purpose, using a low-cost biosorbent made from durian husk and Evans blue (EB) dye as a subject. The EB dye adsorption percentage was determined to be 95.95% with 72.0 mg/g adsorption amount at optimal conditions of pH 2 and 40 °C. The second-order kinetic model fit the experimental data the best. Additionally, the results indicated that the Sips isotherm model fits the experimental data better and that the experiment involved single-layer adsorption on the adsorbent surface. A non-linear regression of the van't Hoff plot gave negative values of Gibbs free energy (−39.38 to −41.48 kJ/mol) at all the temperatures studied (from 20 to 60 °C), indicating that the adsorption process is spontaneous and feasible. A negative value for the enthalpy (ΔH^o=−23.37 kJ/mol) indicated that the adsorption was exothermic, and the positive value of (ΔS^o=54.55 kJ/mol·K) concludes the nature of adsorption of Evans blue dye by Durian husk likely to follow a physisorption adsorption mechanism.

Keywords: Biosorption, Durian Husk, Evans Blue Dye, Non-linear Regression, Thermodynamics

INTRODUCTION

The textile industry's industrial wastewater is one of the most significant causes of environmental contamination; its composition is complicated, contains both organic and inorganic pollutants, and a variety of colors. Dyes can be classified as acid, active, basic, dispersion, diazo, azo, and anthraquinone dyes based on their chromophore structure [1]. Of the 900,000 metric tons of dyes generated each year, 70% are classified as azo dyes [2]. Azo dyes have a negative impact on both human health and the environment. Evans blue dye is classified as a diazo dye due to the presence of two azo bonds in the molecule [3]. It is heavily used in South East Asia including Malaysia in the Batik textile industry and represents significant pollution [4]. Because of its cheap starting costs, ease of design, high effectiveness, and total elimination of contaminants from aqueous solutions, biosorption in environmental engineering is a growing market for pollution remediation globally. Biosorption is one possible approach for dye removal in aquatic environments [4-6]. Durian (*Durio zibethinus*), often known as the "king of fruits", is a dicotyledonous species of plant that is a family of the Bombacaceae and the genus Durio. It is indigenous to Southeast Asia. Durian is one of Malaysia's favorite seasonal fruits. Due to the abundance of sources during its season, it has become a prominent agricultural waste in Malaysia. Environmentalists are now concerned about the trash generated by durian consumption. In addition to being quite heavy owing to the weight of the prickly husk, the trash also emits a very strong and pungent odor that may affect the surrounding life [7]. These durian husks waste can consequently be utilized to derive more economic value while at the same time overcoming environmental problem since the soft and spongy texture of the inner durian shell makes it an excellent adsorbent for many toxicants, including dye [8-13]. Evans blue is a toxic compound [14-16] that forms a significant pollutant in the textile industry, of which several studies for its removal via biodegradation have been reported globally [4-6,17]. In this study, we demonstrate the utility of durian husk in the adsorption of the dye Evans Blue for the first time.

MATERIALS AND METHODS

Evans blue dye (EB) with a purity of 99.9% was sourced from

†To whom correspondence should be addressed.
E-mail: mohdyunus@upm.edu.my

Sigma Aldrich, USA. A 500 mg L^{-1} dye stock solution was prepared in distilled water.

1. Preparation of Durian Husk Biosorbent

Durian husk was freshly collected from the roadside stall near Bangi, Selangor. The husks were first washed with copious volume of distilled water to discard of any impurities. Drying of the husk was carried out at 110 °C for 24-48 h in a hot air oven. The determined weight of durian husk was soaked for 24 h in 1 M KOH solution to the ratio of 1 : 1 (w : v) [18]. The husk was washed with copious amount of distilled water and then dried as before. It was pulverized in a laboratory grinder, rinsed with distilled water, and dried. Ground biosorbent was sized by passing through a British standard sieve (BSS) with a mesh of 18 (1000) Then, the KOH-treated durian husk was sealed in zip lock containers for further experiment.

2. Characterization of Durian Husk Biosorbent

The surface morphology of the biosorbent was characterized using Field-emission scanning electron microscope (FESEM) while Fourier transform infrared spectroscopy (FTIR) was used to determine the surface functional groups of the biosorbent. The determination of the point of zero charge pH_{pzc}, 0.5 g of the biosorbent was introduced to 50 mL of 0.1 M NaCl. The pH adjustment from 2 to 12 was carried out using 0.1 M NaOH or 0.1 M HCl. After 24 h of equilibrium, the final pH was determined (pH_f). The graph shows the relationship between pH_i and pH_f, where pH is found to be significant between both the initial and final pH ($pH_i - pH_f$) [19].

3. Batch Adsorption Study

Batch adsorption studies including several adsorption parameters such as the effect of pH, initial dye, the adsorbent dosage, dye biosorbent contact time, agitation speed and temperature [20]. The amount of dye remaining in the solution was centrifuged at 10,000 x g for 10 min and the supernatant was measured at 540 nm using uv-vis spectrophotometer at equilibrium, the parameter q_e (mg/g) was calculated as:

$$q_e = \frac{(C_0 - C_e)}{W} V \tag{1}$$

where V is volume (L), C_0 and C_e (mg/L) are the initial and at equilibrium, respectively, of the liquid-phase concentrations of adsorbate (mg/L) and W is the mass (g) of the adsorbent used.

4. Response Surface Methodology Optimisation

The Design-Expert software was utilized to analyze the response surface methodology (Stat-Ease Inc., Minneapolis, USA). The Box-Behnken experimental design for Set 1 and 2 was prepared as shown in Tables 1 and 2, respectively.

The regression model is built to:

$$Y = a_0 + \Sigma_{i=1}^{3} a_i X_i + \Sigma_{i=1}^{3} a_{ii} X_i^2 + \Sigma_{i=1}^{3} \Sigma_{j=i+1}^{3} a_{ij} X_i X_j \tag{2}$$

Table 1. Levels of the independent variables (Set 1)

Independent variables	Factor	Coded levels		
		−1	0	+1
Initial concentration (mg/L)	A	50	75	100
Adsorbent dosage (g/L)	B	1	5.5	10
Contact time (h)	C	5	14.5	24

Table 2. Levels of the independent variables (Set 2)

Independent variables	Factor	Coded levels		
		−1	0	+1
Initial concentration (mg/L)	A	50	75	100
pH	B	2	3	4
Agitation speed (rpm)	C	0	75	150

where Y, the constant is a_0, the linear coefficient is a_i, the secondary coefficient is a_{ii}, the interaction coefficient is a_{ji}, and the independent variables are X_i and X_j. To assess the model significance, the fitting excellence test (R^2 test) is chosen.

5. Kinetics, Isotherm, and Thermodynamic Models

This approach is like the one used in batch equilibrium investigations. The concentration of the solution of the absorbent-absorbate solution at various time intervals was determined. The quantity of adsorbed at time t, denoted by the symbol q_t (mg/g), was estimated using Eq. (3). q_t denotes as the adsorption capacity by 1 gram of adsorbent at certain time of exposure. The adsorption rate is assumed to be proportional to the difference between the adsorbed concentration and the number of accessible sites in the pseudo-first-order equation (PFO) proposed by Lagergren for solid-liquid systems [21]. A second-order relation between the adsorption rate and the difference between saturation concentrations is proposed in the pseudo-second-order model (PSO), which implies that chemisorption is the rate-limiting step [22].

5-1. Equation for Pseudo-first-order Kinetic Model

The pseudo-first-order kinetic model equation is as follows [23]:

$$q_t = q_e(1 - e^{-k_1 t}) \tag{3}$$

5-2. Equation for Pseudo-second-order Kinetic Model

The pseudo-second-order equation is as follows [24]:

The model is based on the adsorption capacity onto a solid phase [24] and the nonlinear form of PSO was initially proposed by Blanchard et al. [25]. It is expressed as:

$$q_t = \frac{k_t q_e^2 t}{1 + k_2 q_e t} \tag{4}$$

The slope and intercept of the plot of t/q_t vs. t give the values of q_e and k_2, respectively.

5-3. Elovich Kinetic Model

The Elovich equation was originally developed to simulate the adsorption of carbon monoxide on the sorbent manganese dioxide. The Elovich model [26] is expressed as follows:

$$\frac{dq}{dt} = a\exp(-bq_t) \tag{5}$$

where b is surface coverage extent (g mg^{-1}) and chemisorption activation energy and a is the initial sorption rate (mg g min^{-1}).

For the biosorption isotherms, 17 isotherms models (Table 3) were utilized covering from one to five parameters models, and nonlinear regression instead of linear regression was carried out and the best model assess using several error function analyses listed below. For the thermodynamic calculations, a dimensionless equilibrium constant was estimated from the Langmuir equation [27].

Table 3. Isotherm models utilized in this study

	Model	Formula
1	Henry's law	$q_e = HC_e$
2	Langmuir isotherm	$q_e = \frac{q_{mL} b_L C_e}{1 + b_L C_e}$
3	Freundlich isotherm	$q_e = K_F C_e^{\frac{1}{n_F}}$
4	Temkin isotherm	$q_e = K_F C_e^{\frac{1}{n_F}}$
5	Jovanovic isotherm	$q_e = \frac{K_s q_{mS} C_e^{\frac{1}{n_S}}}{1 + K_s C_e^{\frac{1}{n_S}}}$
6	Redlich-Peterson isotherms	$q_e = \frac{K_{RP} C_e}{1 + \alpha_{RP} C_e^{\beta_{RP}}}$
7	Sips isotherm	$q_e = \frac{K_s q_{mS} C_e^{\frac{1}{n_S}}}{1 + K_s C_e^{\frac{1}{n_S}}}$
8	Toth isotherm	$q_e = \frac{q_{mT} C_e}{(K_T + C_e^{n_T})^{n_T}}$
9	Hill isotherm	$q_e = \frac{q_{mH} C_e^{n_H}}{K_H + C_e^{n_H}}$
10	Khan isotherm	$q_e = \frac{q_{mK} b_K C_e}{(1 + b_K C_e)^{a_K}}$
11	BET isotherm	$q_e = \frac{q_{mBET} \alpha_{BET} C_e}{(1 - \beta_{BET} C_e)(1 - \beta_{BET} C_e + \alpha_{BET} C_e)}$
12	Vieth-Sladek isotherm	$q_e = \frac{q_{mVS} b_{VS} C_e}{(1 + b_{VS} C_e)^{n_{VS}}}$
13	Fritz-Schlunder-III isotherm	$q_e = \frac{q_{mFS} K_{FS} C_e}{1 + q_{mFS} C_e^{n_{FS}}}$
14	Unilin isotherm	$q_e = \frac{q_{mU}}{2b_U} \ln\left(\frac{a_U + C_e e^{b_U}}{a_U + C_e e^{-b_U}}\right)$
15	Baudu isotherm	$q_e = \frac{q_{mB} b_B C_e^{(1+x+y)}}{1 + b_B C_e^{(1+x)}}$
16	Marczewski-Jaroniec isotherm	$q_e = q_{mMJ}\left(\frac{(K_{MJ} C_e)^{n_{MJ}}}{1 + (K_{MJ} C_e)^{n_{MJ}}}\right)^{\frac{m_{MJ}}{n_{MJ}}}$
17	Fritz-Schlunder-IV isotherm	$q_e = \frac{A_{FS} C_e^{a_{FS}}}{1 + B_{FS} C_e^{b_{FS}}}$

Thermodynamics parameter analysis

The Langmuir equation (Eq. (6)) was utilized to find the dimensionless equilibrium constant between two phases, K_L.

$$q_e = \frac{q_{mL} K_L C_e}{1 + K_L C_e} \tag{6}$$

The K_L value from Langmuir was then converted to a dimensionless form K_C using Eq. (7) as follows [27]:

$$K_C = 980.6 \times 55.5 \times 1{,}000 \times K_L \tag{7}$$

The molecular weight of Evans blue is 980.6 $gmol^{-1}$. 55.5 is the molarity of pure water and the term of $980.6 \times 55.5 \times 1{,}000 \times K_L$ will be dimensionless.

The dimensional constant K_L relation to the unitless equilibrium constant of K_C is described in Eq. (8) where, C^o is the selected standard of adsorbate (C^o=1 mol/L); K_L (L/mol) is the Langmuir constant and γ (dimensionless) is the activity coefficient of adsorbent in solution [27].

$$K_C \approx \frac{K_L\left(\frac{L}{mol}\right) \times C^o\left(\frac{mol}{L}\right)}{\gamma} \tag{8}$$

The van't Hoff equation was applied to determine the adsorption thermodynamics parameters (ΔG^o, ΔH^o and ΔS^o). The free energy change (ΔG) is nearly zero when the adsorption process reaches equilibrium. Then, Eq. (9) becomes the standard Eq. (10) which is routinely used to compute ΔG^o (standard Gibbs energy change) while Eq. (11) is the corresponding nonlinear form.

$$\Delta G^o = -RT \ln K_C \tag{9}$$

$$\ln K_C = \frac{-\Delta H^o}{R} \times \frac{1}{T} + \frac{\Delta S^o}{R} \tag{10}$$

$$K_C = e^{\frac{\Delta S}{R} - \frac{\Delta H}{R} \cdot \frac{1}{T}} \tag{11}$$

The universal gas constant, R is 0.00831 kJ/mol×K.

The connection among ΔG^o, ΔH^o and ΔS^o of an adsorption process is expressed as follows:

$$\Delta G^o = \Delta H^o + \Delta S^o \tag{12}$$

6. Statistical Analysis

For all models tested in this study, statistical discriminatory tests such as root-mean-square error (RMSE), corrected AICc (Akaike Information Criterion), accuracy factor (AF) and bias factor (BF) and adjusted coefficient of determination (R^2) were utilized in this work. All the parameter estimations were made using CurveExpert 6.0.

The RMSE was calculated according to Eq. (13) where n is experimental datapoints, Ob_i and Pd_i are the experimental and predicted data, respectively, while p is parameter numbers.

$$RMSE = \sqrt{\frac{\sum_{i=1}^{n} (Pd_i - Ob_i)^2}{n - p}} \tag{13}$$

Since R^2 ignores models' parameter numbers, the adjusted R^2 is commonly used as it has penalty for number of parameters. In the equation (Eqs. (14) and (15)), the total variance of the y-variable is denoted by S_y^2 while RMS is the Residual Mean Square.

$$\text{Adjusted}(R^2) = 1 - \frac{RMS}{s_y^2} \tag{14}$$

$$\text{Adjusted}(R^2) = 1 - \frac{(1 - R^2)(n - 1)}{(n - p - 1)} \tag{15}$$

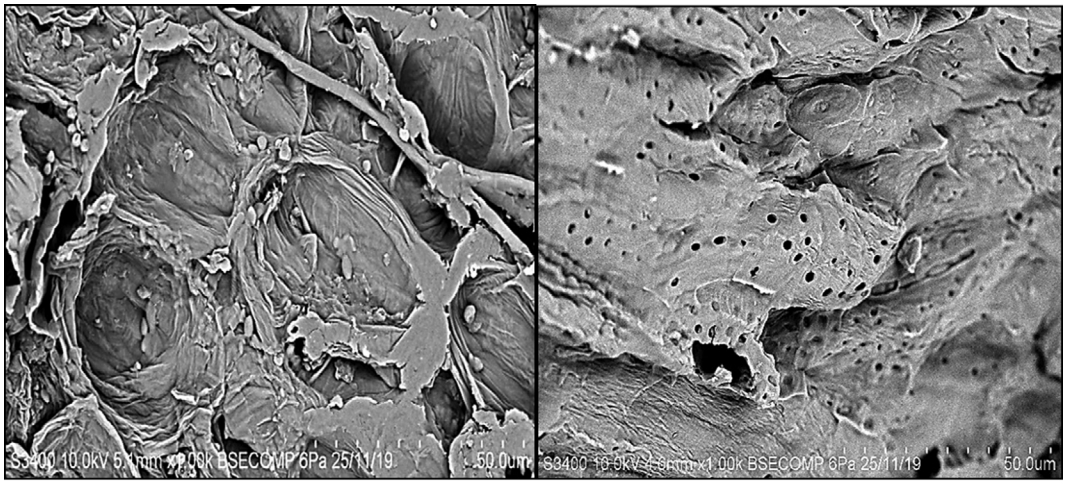

(a) (b)

Fig. 1. SEM micrograph of raw durian husk after 48 h drying at 110 °C (a). Development of pores of durian husk after chemical modification using 1 M of KOH (b).

The Akaike Information Criterion (AIC) AICc, which is based on the information theory [28] is calculated as follows (Eq. (16)).

$$AICc = 2p + n\ln\left(\frac{RSS}{n}\right) + 2(p+1) + \frac{2(p+1)(p+2)}{n-p-2} \quad (16)$$

Further error function analysis are the Accuracy Factor (AF) and Bias Factor (BF). (Eqs. (17) and (18)).

$$\text{Bias factor} = 10^{\left(\sum_{i=1}^{n} log\frac{(Pd_i/Ob_i)}{n}\right)} \quad (17)$$

$$\text{Accuracy factor} = 10^{\left(\sum_{i=1}^{n} log\frac{|(Pd_i/Ob_i)|}{n}\right)} \quad (18)$$

RESULTS AND DISCUSSION

1. Durian Biosorbent Characterization

Based on SEM, the durian husk was porous with a honeycomb-like structure Fig. 1(a). This structure is following the durian husk morphology observed in previous studies [20,29-31]. Further modification of the durian husk surface using concentrated KOH enhanced the porosity of the adsorbents as shown in Fig. 1(b).

Table 4 shows the proportion of C, H, N, S, and O components in durian husk green biosorbent before and after adsorption. Durian husk has a high carbon content, which makes it a good biosorbent when transformed into activated carbon for future adsorption studies [31]. The increase in nitrogen and sulphur after adsorption shows that the EB dye was adsorbed on the adsorbent surface This increase of these elements proves the capabilities of durian composition as good biosorbent for dye as well as organic metal chelation [32]. Also, Fig. 2 shows a significant carbon content in durian husk from SEM-EDX spectrum.

Table 4. Elemental analysis of durian husk before and after EB dye adsorption process

	Control adsorbent	Treated adsorbent
C [%]	44.97	42.63
H [%]	5.18	5.34
N [%]	1.05	10.64
S [%]	5.2	12.73
O [%]	43.6	28.66

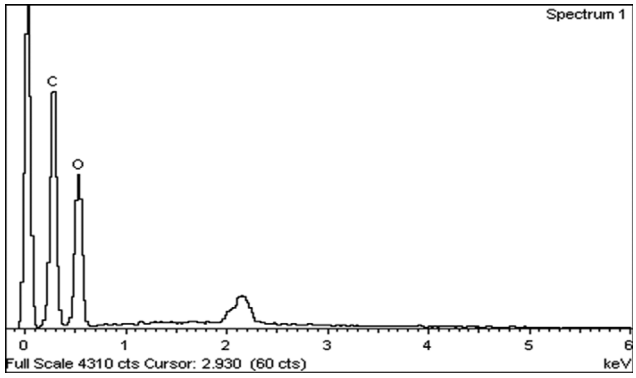

Fig. 2. SEM-EDX of elements content in durian husk.

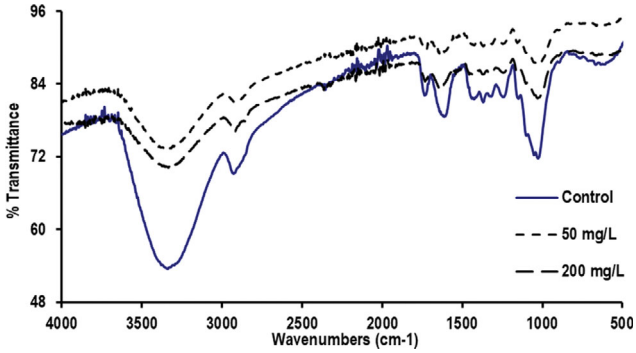

Fig. 3. Comparison of FTIR spectrum of the durian husk before and after treatment for EB with concentration of 50 mg/L and 200 mg/L.

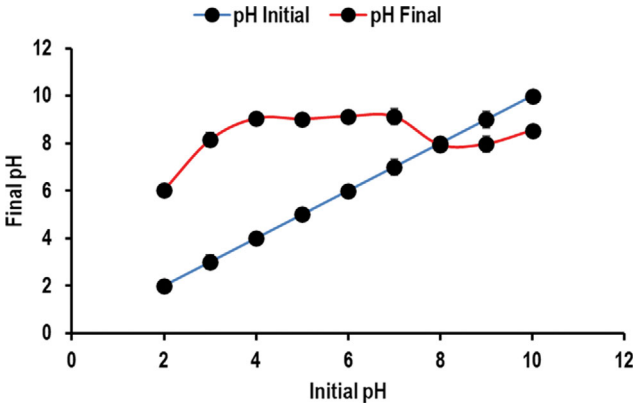

Fig. 4. The plot of ΔpH against the initial pH of durian husk adsorbent surface in determining the point of zero charge of the adsorbent. Error bars represent mean±standard error (n=3).

FTIR has qualitatively observed the presence of large functional groups on the surface of the durian husk (Fig. 3). For the control, a strong peak 3,338.22 cm^{-1} indicates hydrogen bonding of the lignocellulosic component in durian husk [20]. Through π-π interaction and hydrogen bonding creation, functional components containing oxygen frequently play a interacting role in reacting with aromatic pollutants in [33]. The peak at 2,920.7 cm^{-1} is related to the vibration of the aliphatic group, alkane (CH_3). Shifting of C=O bond can be seen at 2,855.1 to 2,850 cm^{-1}. Carboxyl group was observed at 1,733 cm^{-1}. Alkenyl C=C bond was observed at 1,609.33 cm^{-1}. The interaction between hydroxyl and carboxyl groups on the surface of durian husk biosorbent helps in the removal of EB dye from water bodies, and observations are reported in previous studies of the dye adsorption process [20,34].

2. Point of Zero Charge Study

The present study shows that pH_{pzc} of durian husk is at pH 4 as illustrated in Fig. 4. pH_{pzc} is the condition where the solution's surface charge density is equal to zero [20,34]. The present result is in accordance with previous studies utilising several agricultural by-products as a low cost biosorbent.

3. Batch Adsorption Optimization and Response Surface Methodology

Through one-factor-at-a-time (OFAT) and response surface methodology (RSM), a batch adsorption experiment was carried out to examine EB dye sorption parameters such as pH, contact time, initial concentration, adsorbent dose, particle size, agitation speed, and temperature. The graph of the effects of all the tested parameters is presented in Fig. 5. Each of the optimized parameters was carried forward throughout the study. The study of contact time presents an increase in adsorption amount with increase in adsorbate concentration. At the initial point of the first 5 min, adsorption occurred rapidly as there are more vacant sites on the adsorbent surface to be occupied with dye molecules. Adsorption at various dye concentrations was rapid in the beginning and then gradually decreased as adsorption progressed until equilibrium was attained (Fig. 5(a)). Fig. 5(b) shows the effect of adsorbate pH. In this study, the maximum adsorption of EB dye by durian husk biosorbent is at pH 2 with 92% of removal percentage and 47.22 mg/g adsorption capacity. There is no significant difference of adsorption between pH 1 and 2 as it shows that EB dye favours the lower and acidic pH condition to perform high adsorption capacity. The maximum concentration of 75 mg/L can be adsorbed by durian husk with 94.1% of removal percentage were showed in Fig. 5(c). Because a particular mass of sorbent material may only adsorb a certain amount of dye, the initial dye concentration of an effluent is critical. To test the effect of initial dye concentration, an adsorbent - adsorbate solution with a fixed adsorbent dose and varying initial dye concentrations for different time intervals was prepared and shaken until equilibrium was reached. Fig. 5(d) shows an insignificant fluctuation of adsorption capacity upon increasing the dosage up to 10 g/L. The unstable increment at the lower adsorbent dosage is due to the weak binding of the dye sorbate molecule with the adsorbent binding sites. Conversely, the adsorption amount of EB dye by durian husk shows a downward trend after increasing in the biosorbent dosage from 10 to 50 g/L. Fig. 5(e) and (f) depict the study of agitation and temperature effect on the EB dye removal, which show the highest removal percentage at 50 rpm and 303.15 K (30 °C), respectively. Adsorption decreased with increasing temperature, showing that the adsorption process requires less energy to complete. The effect of temperature on the adsorption process was further explored via thermodynamics parameters to finalize the feasibility and spontaneity of the adsorption process.

Based on the Plackett-Burman screening, the parameters contact duration, starting concentration, and adsorbent dose were determined to be important and were then subjected to RSM optimization using the Box-Behnken design. In comparison, results from OFAT and RSM were summarized and compared to each other as shown in Table 5. A better comparison was achieved through RSM optimization. The ultimate ideal circumstances were pH 2, 75 mg/L of EB dye with an adsorption quantity of 72.0 mg/g within 5 h of equilibrium time, utilising an adsorbent dose of 10 g/L at 303.15 K.

ANOVA (Table 6) supported the BB model's adequacy for experi-

Table 5. OFAT and RSM for dye adsorption onto durian husk

Factors		OFAT		RSM	
		Adsorption capacity (mg/g)	Removal percentage (%)	Adsorption capacity (mg/g)	Removal percentage (%)
pH	2	67.90	93.24	72.00	96.00
Initial concentration	75 mg/L				
Dosage	10 g/L				
Agitation speed	75 pm				

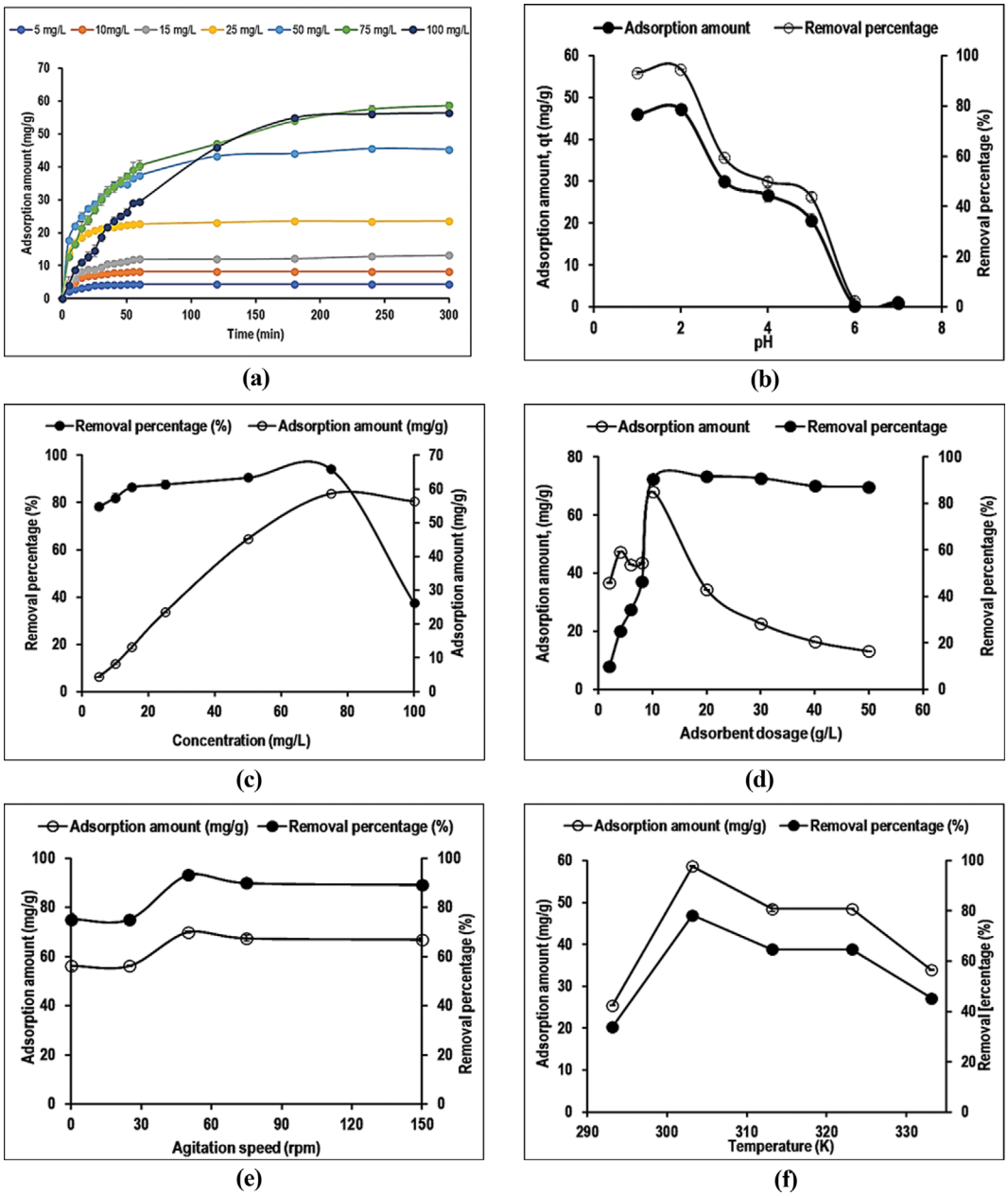

Fig. 5. Effect of contact time (a), pH (b), dye concentration (c), adsorbent dosage (d), agitation speed (e), temperature (f) on the biosorption of several concentrations of EB dye on durian husk biosorbent. Error bars represent mean±standard error (n=3).

mental set 1, with F-value of 27.55 and p-value of 0.0001. A, B, C, A^2, B^2, C^2, and AB are important model terms here. The AB model implies significant interaction between separate components. A high connection exists between the experimental R^2 (0.9755) and the adjusted R^2 (0.9372). "Adeq Precision" ratio of 14.847 indicates a good signal. The CV% was 14.53, which is noteworthy. The PRESS value was 3699.43. Multiple regression analysis revealed a second-order polynomial equation (h) representing EB dye sorption (Y).

$$Y=+65.96-21.69A+12.30B-5.41C-28.10A^2-8.37B^2-10.75C^2-8.94AB+0.056AC+3.66BC$$

Fig. 6 shows the 3D response surfaces and contour plots of the model of the interactions between significant independent variables (A) initial EB dye concentration, (B) durian biosorbent dosage, and (C) contact time towards dependent variable, removal percentage of EB dye from experimental design (Set 1). The interaction between the initial concentration of EB dye (A) and adsorbent dosage (B) on EB dye percentage removal with the constant value of contact time (B) is depicted in Fig. 6(a). The highest EB dye removal was found between 50 and 75 mg/L and the mass of adsorbent dosage at 7 to 10 g/L results in 80% of EB dye removal. The elliptical shape of the 3D wired frame and contour plot indicates the mutual interaction between independent factors was a

Table 6. ANOVA result (Set 1) of the quadratic model of EB dye removal percentage by durian husk

Source	Sum of squares	DF	Mean square	*F*-value	Prob >*F* (*p*-value)	
Model	10,008.06	9	1,112.01	27.55	<0.0001	Significant
Residual	282.59	7	40.37			
Lack of fit	225.65	3	75.22	5.28	0.0708	Not significant
Pure error	56.93	4	14.23			
Cor total	10,290.65	16				
Standard deviation	6.35		R^2		0.9725	
Mean	43.73		Adjusted R^2		0.9372	
C.V.	14.53		Predicted R^2		0.6405	
PRESS	3,699.43		Adeq Precision		14.847	

Note: A: Initial concentration (mg/L), B: Biosorbent dosage (g/L), C: Contact time (hr)

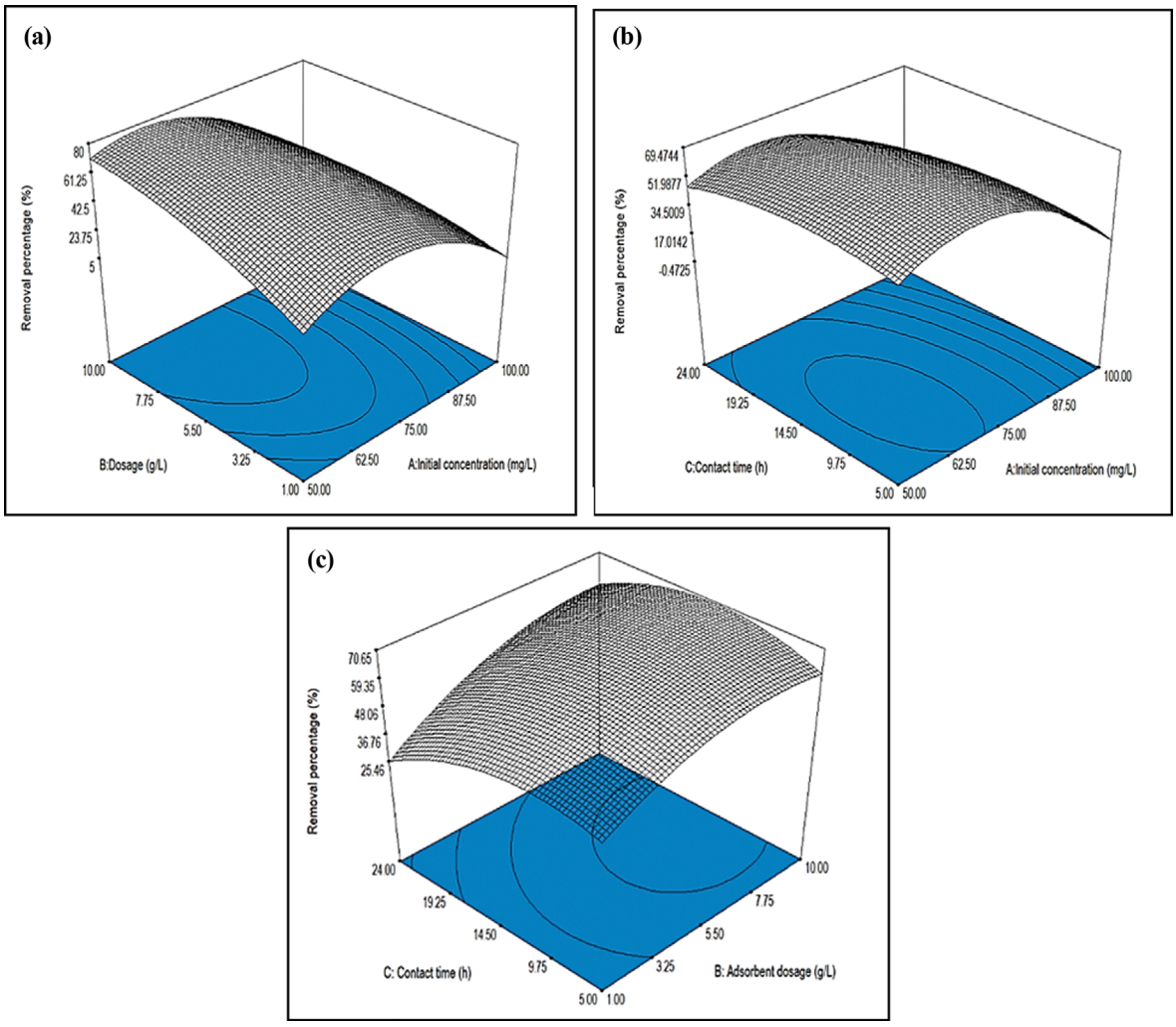

Fig. 6. The 3D response surface plots of the interactions between significant independent variables (a) initial EB dye concentration, (b) Durian biosorbent dosage, and (c) contact time towards dependent variable, removal percentage of EB dye from experimental design (Set 1).

significant response surface model [35]. Fig. 6(b) illustrates the interactive terms of AC showing the effect of independent factors of initial concentration (A) and contact time (C) toward the response, removal percentage of EB dye with the constant adsorbent dosage (B). The highest percentage of EB dye removal was achieved at the concentration of 75 mg/L adsorptions within 14.5 h of equilibrium

contact time. The elliptical shape describes the interaction between factor A and C, which results in the maximum percentage of EB dye removal, 70%. With the initial concentration remaining constant at 75 mg/L, the highest EB dye removal of 75% was obtained when increasing in adsorbent dosage with a minimum equilibrium contact time of 5 h.

Table 7. ANOVA result (Set 2) of the quadratic model of EB percentage removal by durian husk

Source	Sum of squares	DF	Mean square	*F*-value	Prob >*F* (*p*-value)	
Model	13,163.34	9	1,462.59	151.16	<0.0001	Significant
Residual	67.73	7	9.68			
Lack of fit	49.90	3	16.63	3.73	0.1179	Not significant
Pure error	17.83	4	4.46			
Cor total	13,231.07	16				
Standard deviation	3.11		R^2		0.9949	
Mean	32.16		Adjusted R^2		0.9883	
C.V.	9.67		Predicted R^2		0.9376	
PRESS	826.26		Adeq Precision		39.733	

A: Initial concentration (mg/L), B: pH, C: Agitation speed (rpm)

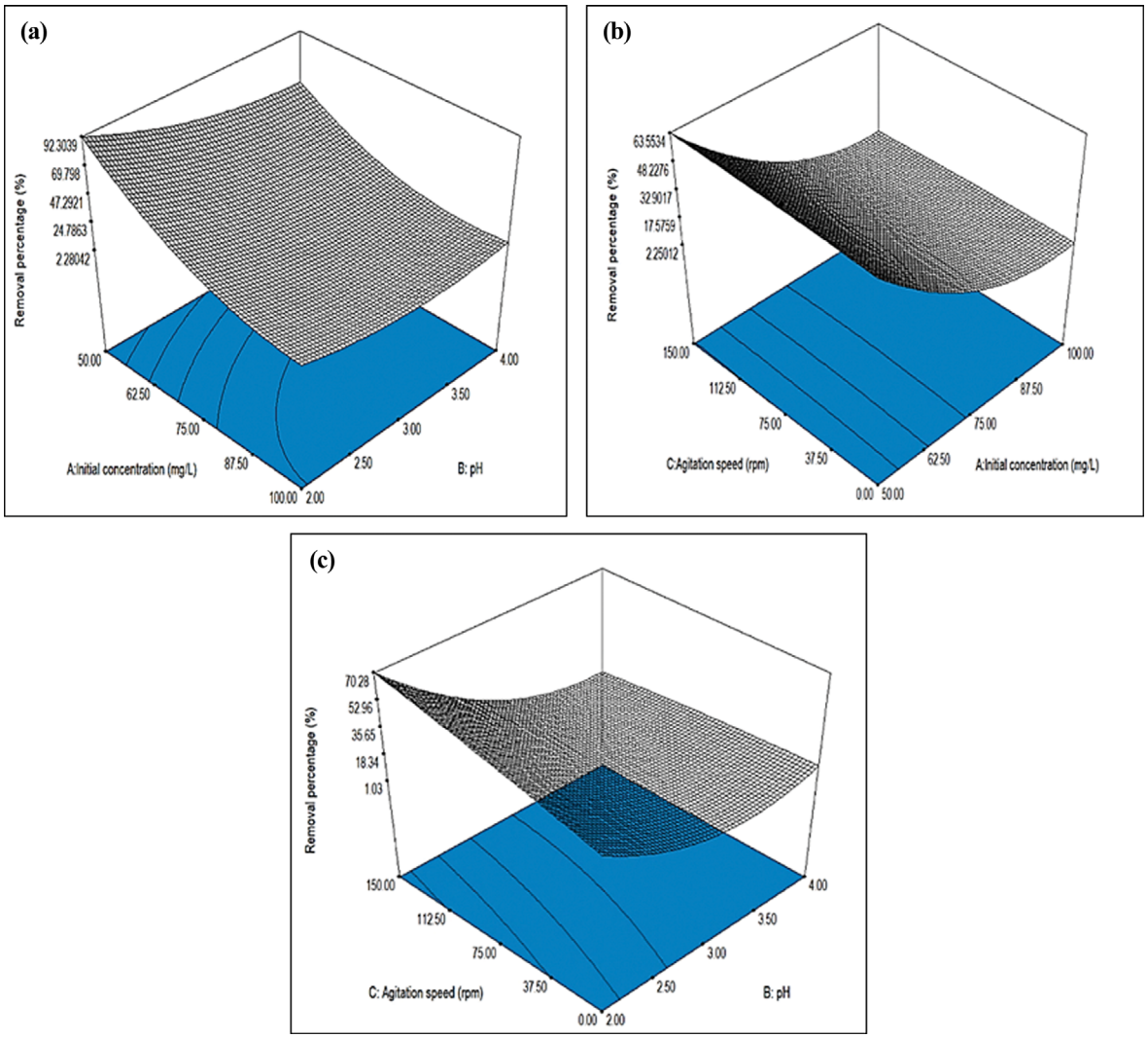

Fig. 7. The 3D response surface plots of the interactions between significant independent variables (a) initial EB dye concentration, (b) pH, and (c) agitation speed towards dependent variable, removal percentage of EB dye from experimental design (Set 2).

ANOVA (Table 7) was used to assess the BB model's adequacy in Set 2, and the model with an F-value of 151.16 and a *p*-value of 0.0001 was found to be statistically significant. The computed experimental R^2 was 0.9949, which had a strong agreement with both the adjusted R^2 (0.9883) and the projected R^2 (0.9376). The "Adeq Precision" ratio of 39.733 suggests that the signal is adequate. The coefficient of variation per cent was 9.67, which is relatively good. The data was subjected to multiple regression analysis, with the resulting second-order polynomial Eq. (9) in terms of coded level reflecting EB dye elimination % (Y).

$$Y=+12.76-21.42A-24.18B+5.38C+23.65A^2+18.75B^2-1.18C^2 -4.83AB-1.60AC-10.39$$

For Set 2, Fig. 7 shows the 3D response surfaces and contour plots of the model of the interactions between significant independent variables (A) initial EB dye concentration; (B) pH, and (C) agitation speed towards the dependent variable, removal percentage of EB dye from the experimental design. The interaction between the initial concentration of EB dye (A) and pH (B) on the adsorption amount of EB dye at a constant speed (C). The highest adsorption amount was found at 50 mg/L and the lowest point was pH 2, which results in 95.45% EB dye removal (Fig. 7(a). Fig. 7(b) illustrates the interactive terms of AC showing the effect of independent factors such as initial concentration (A) and contact time (C) toward the response, and the adsorption amount of EB dye with the constant pH 2 (B). The highest percentage of dye removal was obtained with adsorption concentrations of 50 mg/L and the highest point of agitation speed of 150 rpm. The elliptical shape describes the interaction between factors A and C which results in the percentage removal of EB dye, 60.43%. The interaction between the independent parameters of adsorbent dosage (B) and contact time (C) is illustrated in Fig. 7(c). With the constant initial concentration of 75 mg/L, the removal of EB dye, which is 70.28%, was obtained when decreasing in pH with the increasing agitation speed. The non-elliptical shape of the 3D wired frame and contour plot indicate the least mutual interaction between independent factors was a substantial response surface model [35].

4. Determination of Kinetic Model for Batch Adsorption Studies

Kinetic analysis used three models: pseudo-first order (PFO), pseudo-second (PSO) and Elovich (Fig. 8). Since linearization of nonlinear data disturbs the data's error structure, this makes it harder to assess uncertainty, which is often reported as 95% confidence interval range [36]. Hence, non-linear regression is preferable for kinetic model fitting since it is conducted on the same abscissa with a linear regression plot, showing more accurate calculations.

The estimated parameters of each model are presented in Table 8. Considering the statistical indicators, pseudo-second order is more accurate in describing the biosorption kinetic profiles than PFO and Elovich. Kinetic analysis using the PSO model at 75 mg/L of EB dye gives a value of equilibrium adsorption capacity, q_e of 63.59 mg/g (95% confidence interval (C.I.), 60.71 to 66.47) and a value of the PSO rate constant, K_2 of 0.0005 (95% C.I., 0.0004 to 0.0006). The list of other error functions analysis shows the PSO model gave the best values with the lowest RMSE and AICc, adjusted R^2 nearest to 1.0 and bias and accuracy factors near unity. The adsorption process obeyed the PSO at a lower initial dye concentration. It was inferred that the three kinetics models discovered to be suitable for fitting the current adsorption kinetics data are as follows: Pseudo-second order>Elovich>Pseudo-first order. As far as EB dye biosorption is concerned, the PSO model is the best in the biosorption study using the shell waste from *Theobroma grandiflorum* [3,33].

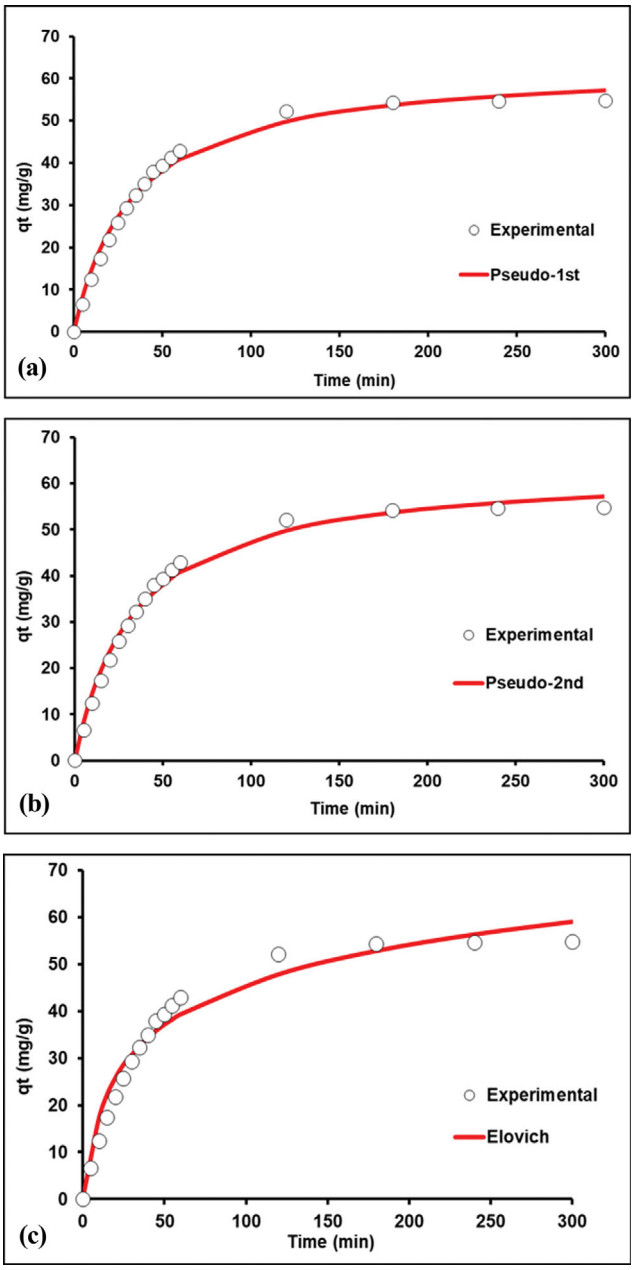

Fig. 8. Kinetics of 75 mg/L EB dye adsorption on durian husk pH 2 as modelled using the Pseudo-first order (a), pseudo-second order (b) and Elovich (c) models.

According to Fig. 9, the pseudo-second order model was utilized to fit data for all EB concentrations, and the data showed excellent agreement with the pseudo-second order equation with all regressed lines showing adjR^2 values >0.98.

It was often accepted that the ability to fit the kinetic data was the best test of the PFO and PSO equations' validity, despite the fact

that such a test has little to do with whether or not the equations have a solid physicochemical foundation. Both k_1 and k_2 were phenomenological rate constants that declined when the adsorbate concentration was raised at the outset. k_1 and k_2 values varied widely from measurement to measurement, making it difficult to draw conclusions about the underlying physics and chemistry and ex-

Table 8. The kinetic parameters of adsorption EB dye onto durian husk adsorbent

Concentration (mg/L)	10	50	75	100
Model				
Pseudo-1st order				
q_e (mg/g)	8.00	41.8	67.80	57.6
k value	0.22509	0.069377	0.107251	0.016426
RMSE	0.4	3.6	0.021	9.4
adR^2	0.96	0.91	0.9764	0.648
AICc	−19.52	53.03	−65.52	85.880
AF	0.99	1.01	1.046	1.143
BF	1.01	1.04	0.995	1.146
Pseudo-2nd order				
q_e (mg/g)	8.40	44.30	54.75	56.1
k value	0.22509	0.069377	0.107251	0.016426
RMSE	0.3	1.8	0.0150	9.3
adR^2	0.98	0.97	0.99	0.677
AICc	−31.34	29.96	−72.71	85.702
AF	1.00	1.00	1.03	1.150
BF	1.01	1.02	1.00	1.160
Elovich				
q_e (mg/g)	9.00	47.8	50.4	56.0
k value (95%, C.I)	0.22509	0.069377	0.107251	0.016426
RMSE	0.6	1.1	0.036	9.7
adR^2	0.91	0.99	0.91	0.601
AICc	−9.48	14.04	−54.87	86.956
AF	0.99	0.99	1.088	1.133
BF	1.04	1.02	0.999	1.138

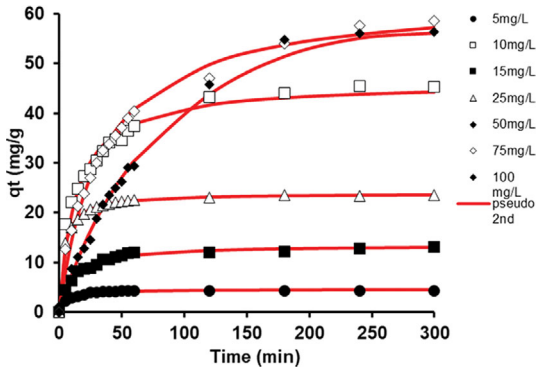

Fig. 9. Experimental data versus calculated data on pseudo-second order kinetic analysis of 75 mg/L EB dye adsorption study.

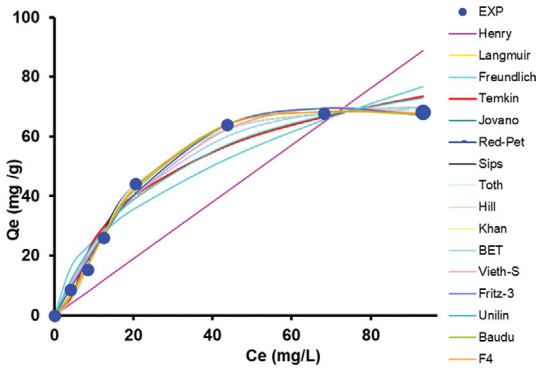

Fig. 10. The summary plot of experimental data and all the selected isotherms models fitted for the EB dye adsorption onto the durian husk biosorbent.

Table 9. Error functions analysis of 17 selected isotherm models of adsorption study

	Model	Parameter	RMSE	R^2	adR^2	AICc	BF	AF
1	Henry	1	1.61	0.75	0.71	14.93	0.67	1.60
2	Langmuir	2	0.49	0.97	0.96	2.27	1.08	1.14
3	Freundlich	2	0.81	0.92	0.88	10.41	1.11	1.23
4	Temkin	2	0.50	0.97	0.96	2.53	0.98	1.16
5	Jovanovic	2	0.27	0.99	0.99	−7.53	1.05	1.08
6	Redlich-Peterson	3	0.21	1.00	0.99	−11.36	1.03	1.05
7	Sips	3	0.20	1.00	0.99	−12.54	0.95	1.04
8	Toth	3	0.22	0.99	0.99	−10.23	1.03	1.06
9	Hill	3	0.20	1.00	0.99	−2.54	0.95	1.09
10	Khan	3	0.29	0.99	0.99	3.82	1.05	1.08
11	BET	3	0.38	0.99	0.97	8.12	1.07	1.11
12	Vieth-S	3	0.29	0.99	0.99	3.83	1.05	1.08
13	Fritz-3	3	0.23	1.00	0.99	−0.02	1.03	1.05
14	Unilin	3	0.54	0.97	0.95	13.64	1.08	1.14
15	Baudu	3	0.14	1.00	1.00	−7.71	0.99	1.05
16	Fritz-4	4	0.15	1.00	1.00	11.69	0.98	1.06
17	Marczweski	4	6.37	1.00	11.69	0.98	1.06	0.00

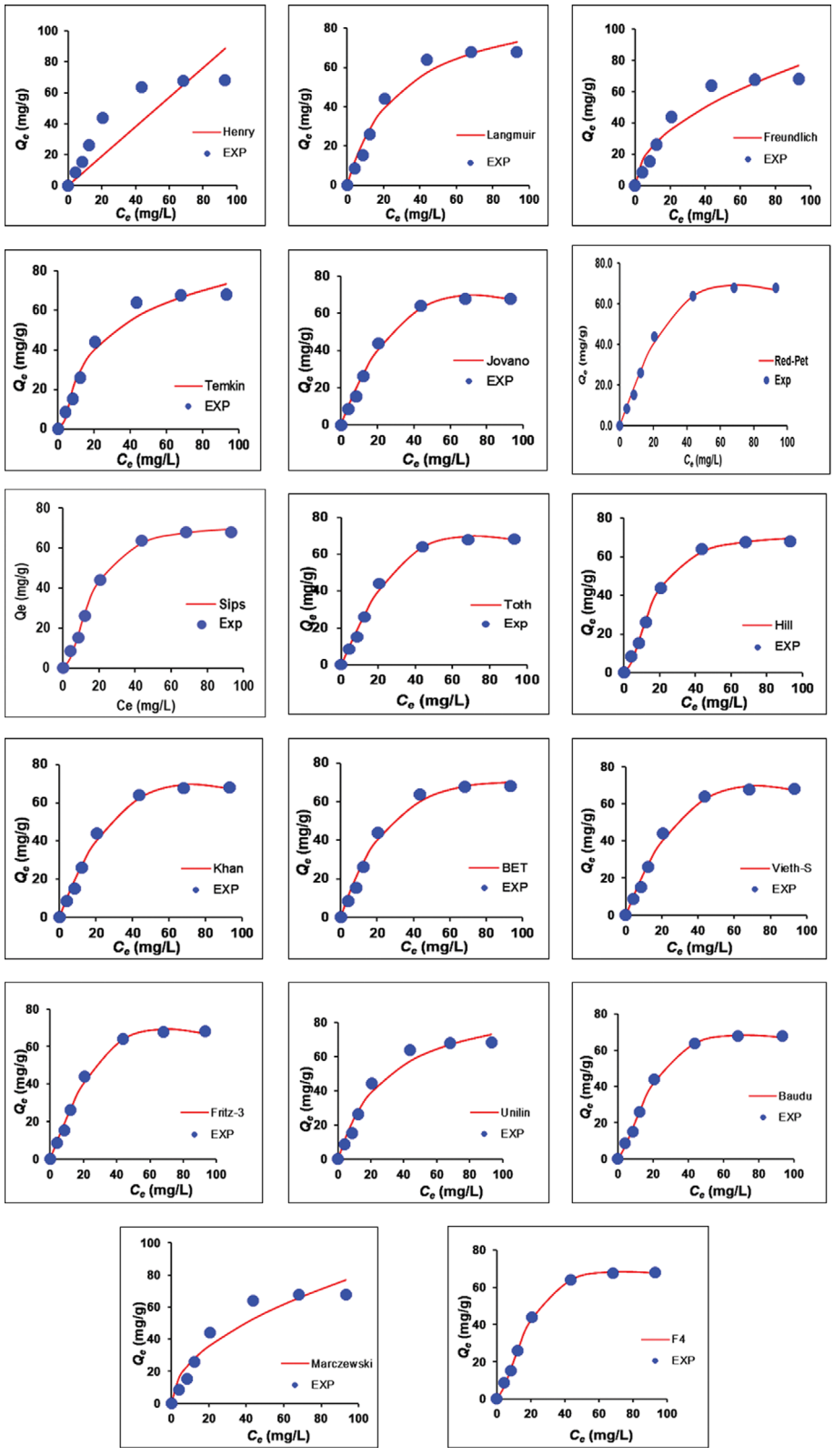

Fig. 11. The equilibrium data of biosorption isotherm fitted to 17 isotherm models.

trapolate valuable results. The PFO and PSO equations may be fitted to most kinetic data even if the experimental conditions affecting the adsorption kinetics were not completely controlled. The PFO equation typically gave lower estimates of q_e than did the experiments. This mismatch was due to a delay in the onset of the adsorption process, which was likely brought on by the existence

Table 10. Sips, Redlich-Peterson, Toth, Jovanovic, Hill model parameters for EB dye adsorption

	Model	Parameter	Value	95% CI Lower	95% CI Upper
1	Sips	q_{mS} (mg/g)	72.029	66.19	77.86
		k_S (l/g)	0.0052	0.000809	0.01129
		n_S	0.5311	0.3968	0.6653
2	Redlich-Peterson	K_{RP1} (l/g)	0.227446	0.1859	0.2689
		α_{RP} (l/mg)	0.000635	0.000105	0.00227
		β_{RP}	1.793568	1.2578	2.3292
3	Toth	q_{mT} (mg/g)	89.81	48.905	67.868
		k_T	9.4663	3.9787	13.914
		n_T	1.540996	1.1155	2.863
4	Jovanovic	q_{mJ} (mg/g)	102.38	96.052	112.65
		K_{J1}	0.00255	−0.3974	0.405
		K_{J2}	−0.01251	−0.20	0.1794
5	Hill	q_{mH} (mg/g)	72.029	66.192	77.864
		n_H	1.8829	1.4068	2.359
		k_H	190.82	85.68	295.44

of boundary layer or external resistance regulating. In the adsorption process that followed the PSO equation, the chemical reaction is not always the rate-limiting step because a good fit alone is not enough to reveal the true nature of the rate-limiting step [37-39].

5. Adsorption Isotherm Model

All 17 isotherms models were fitted to the data (Figs. 10 and 11). Based on Table 9, the Sips isotherm model was found to be the best fit model out of the 17 fitted isotherm models used in the current investigation with an adjusted R^2 value of 0.99, lowest values for RMSE and AICc, while values of accuracy factor (AF) and bias factor (BF) closest to unity. The Sips isotherm is generated by combining both the Langmuir and Freundlich isotherm models in a single equation.

Table 10 is the list of five three-parameter isotherms models out of 17 which have a very good fitting of the experimental result of adsorption data. The best-fit adsorption data was obtained from the Sips isotherm model based on the calculated value of q_{mS}=72.029 mg/g, similar to the actual equilibrium maximum adsorption of experimental data, q_e=72 mg/L. Data on the use of agricultural waste for EB dye removal is scarce with one report is by using the shell waste from *Theobroma grandiflorum* where the maximum adsorption capacity (q_m) was 37.5 mg/g, with the Avrami as the best kinetic model, and incidentally the Sips isotherm also as the best model [33]. In another report using the Aqai stalk a maximum adsorption capacity (q_m) of 46.6 mg/g is obtained with the Avrami as the best kinetic model similar to *Theobroma grandiflorum* and incidentally the Sips isotherm also as the best model [3]. At this point, durian husk is the best agricultural waste biosorbent so far (Table 11). As far as EB dye is concerned, sorption work using other sorption materials is also limited in the literature despite the EB dye being highly used in the textile industry [4,5,17,40].

Theory

Isotherm Studies

Dye molecules in the aqueous phase reach a dynamic equilibrium with those on the adsorbent surface under isothermal conditions during the adsorption process, and this equilibrium is expressed by the isotherms. These adsorption isotherms allow for a straightforward estimation of the optimal loading of adsorbents [41]. The most fitted isotherms, which are system dependent, provide a better explanation of the adsorbent-adsorbate binding. Adsorption equilibrium has been modeled in various ways. The following are explanations of the best isotherm models in this study including the Langmuir and Freundlich models, two models often reported in adsorption studies.

Langmuir

The Langmuir isotherm, assumes that all adsorption sites are the same and have the same energy, and the adsorbent is structurally homoge-neous for monolayer adsorption to occur [42]. This isotherm model predicts the existence of monolayer coverage of the dye at the outer surface of the adsorbent due to the exponential decay of intermolecular forces with increasing distance. This model predicts a constant monolayer adsorption capacity and simplifies to the linear Henry's model for both low and high solute concentrations [43]. Expression of the Langmuir Isotherm is as follows:

$$q_e = \frac{q_{mL} b_L C_e}{1 + b_L C_e}$$

where q_{mL} (mg/g) is the maximum monolayer adsorption capacity predicted by Langmuir isotherm, and b_L (l/mg) (together with q_{mL}) are the Langmuir model constants. Weber and Chakravorti proposed a separation factor (RL) to predict the affinity between the sorbate and sorbent whether it is favorable or unfavorable [44] as follows:

$$R_L = \frac{1}{1 + C_e b_L}$$

An alternative to the Brunauer-Emmett-Teller (BET) method for calculating the surface areas of porous solids is to use the Langmuir isotherm [45]. The BET isotherm model can be reduced to the Langmuir isotherm if the adsorbent surface is assumed to be homogeneous and completely coated by dye molecules. Therefore, the specific surface area S_{sp} (m^2/g) of the adsorbent may be determined using the following equation, which requires knowledge of the maximal monolayer adsorption capacity (q_{mL}) determined using the Lang-

Table 11. Reports of previous study on adsorption of selected dyes by using agricultural wastes

Biosorbent	Dyes	Adsorption capacity	Regression	Best isotherm	Best kinetic	Thermodynamic parameters	Ref.
Modified Durian shell	Methylene blue	410.85 mg/g	Non-linear	Langmuir	Pseudo 2nd	ΔH^o: −1.865 (kJ/mol) ΔS^o: 5.683 (J/molK) ΔG^o: (kJ/mol) 303 K: −0.319 313 K: −0.096 323 K: −0.024 R^2: 0.99 Exothermic	[36]
		49.05 mg/g	Non-linear	Langmuir	Pseudo −1st	-	[58]
	Basic green 4	250 mg/g	Non-linear	-	Pseudo 2nd	-	[59]
	Basic brown 16	77.6%	-	-	-	-	[29]
Durian seed	Methyl red	92.52% 372.46 mg/g	Linear	Freundlich	Pseudo 2nd	ΔH^o: 3.83 (kJ/mol) ΔS^o: 22.84 (J/molK) ΔG^o: (kJ/mol) 303 K: 13.74 318 K: 14.34 333 K: 14.72 Endothermic	[34]
	Remazol brilliant blue reactive	95.17% 357.14 mg/g	Linear	Freundlich	Pseudo 2nd	ΔH^o: 11.98 (kJ/mol) ΔS^o: 17.16 (J/molK) ΔG^o: (kJ/mol) 303 K: 13.08 318 K: 14.16 333 K: 14.16 Endothermic	[34]
Durian shell	Basic brown	77.6%	-	-	-	-	[29]
Jute stick	Methylene blue	142.87 mg/g		Langmuir	-	-	[60]
Prickly pear peel	Methylene blue	260 mg/g	Non-linear	Freundlich	Pseudo 2nd	ΔH^o: 9.66 (kJ/mol) ΔS^o: 82.64 (J/K) ΔG^o: (kJ/mol) 293 K: −33.96 303 K: −34.54 313 K: −35.62 R^2: 0.993 Exothermic	[61]
Palm shell-waste based	Methylene blue	163.3 mg/g		Langmuir Freundlich		-	[62]
Spent coffee ground		986.8 mg/g		Sips		-	[63]
Theobroma grandiflorum shell	Reactive red 192 Direct blue 53	64.1 mg/g 37.5 mg/g	Non-linear	Sips	Avrami	-	[33]

muir equation and the predicted area of a dye molecule A (nm^2).

$$S_{sp} = \frac{6.023 \times 10^{23} \times A \times q_{mL}}{1{,}000}$$

Freundlich Isotherm

When it comes to adsorption, the empirical Freundlich isotherm model is more accurate in describing reality than is the idealized Langmuir isotherm, which is limited to the formation of a monolayer. This relationship helps to explain the phenomenon of multilayer adsorption, in which adsorption heat and affinities are not uniformly distributed over the heterogeneous surface [46,47]. The equation is as follows [47]:

$$q_e = K_F C_e^{\frac{1}{n_F}}$$

in which K_F (l/g) is the Freundlich isotherm constant, and n_F is the

Freundlich exponent. $1/n_F$'s magnitude between 0 and 1 is a measure of the intensity of adsorption or the heterogeneity of a surface; a value below unity indicates a chemisorption process, while a value above 1 denotes cooperative adsorption [46,47].

Jovanovic Isotherm Model

This model's consideration of an adsorption surface assumption is comparable to Langmuir's. A second approximation for localized monolayer adsorption in the absence of lateral interactions corresponds to this scenario. The main difference between this model and the Langmuir model is that in the former, surface binding vibrations of an adsorbed species are taken into account [48]. The equation is as follows [47]:

$$q_e = q_{mJ}(1 - e^{-K_J C_e})$$

Maximal adsorption capacity in the Jovanovic model, expressed in milligrams per gram (mg/g), is denoted by q_{mJ}. Assumptions similar to those of the Langmuir isotherm were used by Jovanovic [48] when he created his model, which additionally took into account the surface binding vibrations of the adsorbed species. One further approximation for lateral-interaction-free monolayer localized adsorption is the Jovanovic isotherm. At very high concentrations, it follows the Langmuir isotherm instead of Henry's law [47]. For Jovanovic local behavior, this isotherm predicts a quasi-Gaussian function with a bias toward high adsorption energies. To get the equivalent Jovanovic equation for multilayer adsorption (three parameters) [48], the equation is as follows:

$$q_e = q_{mJ}(1 - e^{-K_{J1} C_e}) e^{K_{J2} C_e}$$

Redlich-Peterson Isotherm Model

The features of both the Freundlich and Langmuir isotherms are incorporated into the three-parameter model. This model is a mixture of the two, therefore the adsorption mechanism does not follow the rules of ideal monolayer adsorption [49]. Numerous applications exist for the Redlich-Peterson isotherm model, which include homogeneous and heterogeneous systems. The equation is as follows [47]:

$$q_e = \frac{K_{RP} C_e}{1 + \alpha_{RP} C_e^{\beta_{RP}}}$$

where K_{RP} is the Redlich-Peterson model isotherm constant (L/g), α_{RP} is the Redlich-Peterson model constant (mg/L^{-g}), and β_{RP} is the Redlich-Peterson model exponent, which should be in the range (0,1). Redlich-Peterson equation is reduced to the Henry equation at β_{RP}=0 and to the Langmuir equation at β_{RP}=1. Adsorption equilibrium is represented by a linear dependence on concentration, which holds true over a wide concentration range. This is because the numerator is based on the Langmuir isotherm model, which allows it to enter the Henry zone at infinite dilution [50]. To solve the equations, this isotherm model uses a minimal approach. This method optimizes the degree to which the theoretical model's predictions agree with the points in the experimental data [51].

Toth Isotherm Model

Using an empirically modified version of the Langmuir equation, this isotherm model attempts to minimize the discrepancy between the experimental and projected values. This isotherm model is commonly employed for the modeling of heterogeneous adsorption systems, as it adequately accounts for both low and high adsorbate concentrations. This isotherm model assumes a non-normal distribution of adsorption energies, where the majority of sites have energies that are lower than the mean or the peak [52]. The equation is as follows [47]:

$$q_e = \frac{q_{mT} C_e}{(K_T + C_e^{n_T})^{n_T}}$$

where K_T is the Toth isotherm constant and n_T is the Toth isotherm exponent, and q_{mT} (mg/g) is the maximal monolayer adsorption capacity predicted by Toth isotherm. The n_T scale measures the degree of surface variation. It follows from the Langmuir isotherm equation that the process takes place on a homogeneous surface if n_T approaches unity. Therefore, (n_T) is a parameter that represents the heterogeneity of the adsorption system; the system is deemed heterogeneous when (n_T) is not equal to the unity value [53]. Furthermore, as a result of the independent association between temperature and the parameter n_T, an increase in temperature causes a quick increase in K_T.

The Toth isotherm model's equation is preferred over Sips' because it can characterize the data's behavior at both high and low concentrations. Do [54] states that the slope of this isotherm model is constant at zero loading but begins to decrease at a given loading at a pace significantly faster than that for the Langmuir equation. The effect of heterogeneity, as measured by n_T, is responsible for this. As the adsorption process continues, molecules are physically attracted to higher-energy sites, but as the adsorption proceeds, they are attracted to lower-energy sites, resulting in a slower increase in the adsorbed amount vs pressure than that predicted by the Langmuir equation.

Sips Isotherm Model

The Sips isotherm model was developed by fusing the Langmuir and Freundlich isotherm models in order to forecast the heterogeneity of the adsorption systems and to avoid the restrictions associated with the rising concentrations of the adsorbate in the Freundlich model. Next, an expression with a finite limit at high concentration is generated. The Sips model is correct because it effectively localizes the adsorption without involving the adsorbate-adsorbate interaction [55]. The equation is as follows [47]:

$$q_e = \frac{K_s q_{mS} C_e^{\frac{1}{n_s}}}{1 + K_s C_e^{\frac{1}{n_s}}}$$

where K_S (l/g) is the Sips isotherm constant, q_{mS} (mg/g) is the maximum monolayer adsorption capacity by Sips isotherm and n_S is the Sips model exponent. However, the Sips isotherm model deviates from Henry's law since it reduces to the Freundlich model at low adsorbate concentrations. However, the monolayer adsorption feature of the Langmuir model is predicted at high adsorbate concentrations. The equation's parameters are controlled by operational conditions such as changes in concentration, pH, and temperature [56]. The primary flaw of the Sips model is the same as that of the Freundlich model: when pressure (or concentration) is low, neither model predicts the accurate Henry's law limit [54].

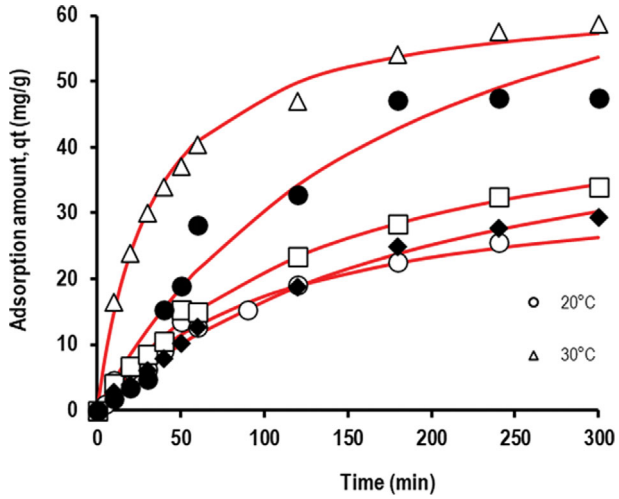

Fig. 12. Kinetic plot of 75 mg/L EB dye adsorption on durian husk biosorbent at various temperatures.

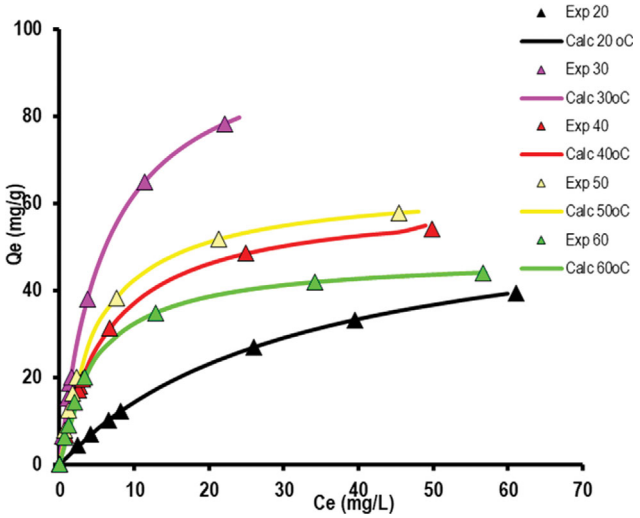

Fig. 13. Langmuir equilibrium adsorption isotherms at various temperature for EB dyes by durian husk biosorbent.

The Hill Isotherm Model

The Hill equation was proposed to explain the binding of various species onto homogeneous substrates, and it derives from the non-ideal competitive adsorption model. The model postulates that the adsorption process is a cooperative event in which the binding ability of a ligand at one site on a macromolecule can affect the binding capacity of other sites on the same macromolecule [57]. The equation is as follows [47]

$$q_e = \frac{q_{mH} C_e^{n_H}}{K_H + C_e^{n_H}}$$

Maximum uptake saturation (in mg/L) as determined by the Hill isotherm, q_{mH}, the Hill constant (K_H), and the Hill cooperativity coefficient (n_H) of the binding interaction (dimensionless). Binding is cooperative if $n_H>1$, non-cooperative or hyperbolic if $n_H=1$, and non-cooperative if $n_H<1$.

Table 12. Thermodynamics parameters calculated from the non-linear plot of van't Hoff and the dimensionless Langmuir constant

T (K)	K_C	ΔG^o (kJ/mol)	ΔH^o (kJ/mol)	ΔS^o (kJ/(mol·K))
293.15	11,163,410	−39.38		
303.15	10,217,862	−40.38		
313.15	8,640,632	−41.04	−23.37	54.55
323.15	8,235,740	−41.44		
333.15	3,786,779	−41.48		

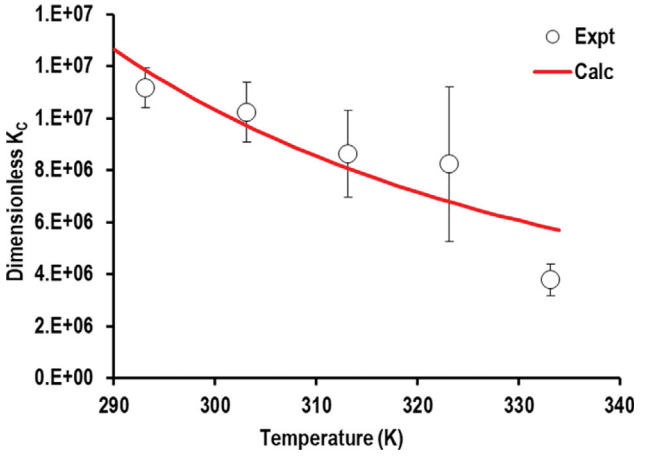

Fig. 14. The nonlinear van't Hoff plot of dimensionless constant, K_C against temperature, K of EB dye adsorption process.

6. Thermodynamic Studies

Fig. 12 depicts the kinetic plot of EB adsorption for different concentrations at different temperature ranges, respectively. The q_e constants from the PSO model were utilized to plot the Langmuir isotherm model to generate the Langmuir constant, K_L.

Fig. 13 depicts the plot of Langmuir isotherms of 75 mg/L EB dyes adsorbed by durian husk at various temperatures.

Table 12 summarizes the results for determining the parameters of thermodynamics. Based on the van't Hoff plot in Fig. 14, the standard Gibbs free energy ($-\Delta G^o$) negative values indicate that the process of EB dye adsorption onto durian husk biosorbent is spontaneous without or with low input of energy and heat [27]. The present study indicates that the adsorption process is likely a physisorption process as adsorption with ΔG^o values ranging from −400 to −80 kJ/mol corresponds to chemisorption. A combination of Sips isotherm as the best model and physisorption or chemisorption as the process governing sorption has been reported in several previous studies that include biosorption metals and dyes [29,64].

The adsorption thermodynamics parameters H^o and S^o were determined, as indicated in Table 12. In general, the van't Hoff plot's slope defines whether the system is endothermic (positive slope) or exothermic (negative slope). As the solution temperature increased from 293.15 to 333.15 K, there appears to be a decrease in the maximum adsorption capacity of EB. This might be due to two possible reasons: a constant increase in widening sorption site on durian husk was unfavorable to an adsorbed dye molecule, and desorp-

tion phenomena produced by weak adsorption contact throughout the adsorption phase [65,66]. The fact that the conventional adsorption enthalpy was negative (H^o=−23.37 kJ/mol) suggests that the adsorption was an exothermic reaction, which agrees with much dye biosorption by agricultural waste works. As far as EB dye is concerned, the two studies using agricultural wastes previously discussed by Cardoso et al. [33] did not present thermodynamic studies in their report. Similarly, other sorbent materials used for EB dye removal [3,67] also did not report thermodynamic studies.

CONCLUSIONS

Durian husk biosorbent is largely made up of irregular and shapeless particles, with sizes on the order of 1 mm with elemental analysis showing the presence of nitrogen, hydrogen, oxygen, and carbon atoms in its amorphous structure. The adsorption of EB dye onto durian husk was more favorable at pH 2. Dye sorption reached equilibrium in 300 min. Statistical analysis implied the pseudo-second order and the Sips isotherm as the best models for kinetics and isotherm, respectively. The maximum biosorption capacity of durian husk for EB was 72 mg g^{-1}. The process was spontaneous, favorable and exothermic. Raw durian husk was able to remove 95.95% of EB dye from an aqueous solution. All these facets suggested that durian husk can be a low-cost biosorbent in the treatment of dye effluents, especially EB dye.

DECLARATIONS

Availability of Data and Materials

Data availability Some or all data, models, or codes generated or used during the study are available from the corresponding author by request.

Competing Interests

The authors declare they have no competing interests.

Funding

This research is funded under the Fundamental Research Grant Scheme (FRGS/1/2019/STG05/UPM/02/7) by the Ministry of Higher Education (MOHE) Malaysia.

Authors' Contributions

The first author Ain Aqilah Basirun did the experiment and wrote a draft of the manuscript, Ahmad Razi Othman, Nur Adeela Yasid, Mohd Izuan Effendi Halmi, Baskaran Gunasekaran, and the corresponding author Yunus Shukor corrected and provide suggestions to improve the manuscript.

REFERENCES

1. F. Tian, Y. Wang, G. Guo, K. Ding, F. Yang, H. Wang, Y. Cao and C. Liu, *Bioresour. Technol.*, **326** (2021).
2. L. A. Adnan, A. R. Mohd Yusoff, T. Hadibarata and A. B. Khudhair, *Water Air Soil Pollut.*, **225** (2014).
3. L. D. T. Prola, E. Acayanka, E. C. Lima, C. Bestetti, W. O. Santos, F. A. Pavan, S. L. P. Dias and C. R. T. Tarley, *Desalination WaterTreat.*, **51**, 4582 (2013).
4. I. K. Chandra, Y.-H. Ju, A. Ayucitra and S. Ismadji, *Int. J. Environ. Sci. Technol.*, **10**, 359 (2013).
5. F. B. D. Saiah, B.-L. Su and N. Bettahar, *Macromol. Symp.*, **273**, 125 (2008).
6. E. Yilmaz, S. Memon and M. Yilmaz, *J. Hazard. Mater.*, **174**, 592 (2010).
7. N. A. Husin, S. Rahman, R. Karunakaran and S. J. Bhore, *Bioinformation*, **14**, 265 (2018).
8. S. M. Anisuzzaman, C. G. Joseph, D. Krishnaiah, A. Bono and L. C. Ooi, *Water Sci. Technol.*, **72**, 896 (2015).
9. Y. Gopalakrishnan, A. Al-Gheethi, M. Abdul Malek, M. Marisa Azlan, M. Al-Sahari, R. M. S. Radin Mohamed, S. Alkhadher and E. Noman, *Sustainability*, **12**, 8928 (2020).
10. M. K. Dahri, L. B. L. Lim, N. Priyantha and C. M. Chan, *Int. Food Res. J.*, **23**, 1154 (2016).
11. S.-T. Ong, S.-Y. Tan, E.-C. Khoo, S.-L. Lee and S.-T. Ha, *Desalination Water Treat.*, **45**, 161 (2012).
12. Z. M. Lazim, T. Hadibarata, M. H. Puteh and Z. Yusop, *Water Air Soil Pollut.*, **226** (2015).
13. Z. M. Lazim, T. Hadibarata, M. H. Puteh, Z. Yusop, R. Wirasnita and N. Mohd Nor, *Jurnal Teknologi*, **74**, 109 (2015).
14. A. M. Malaowalla and C. Fong, *Oral Surgery, Oral Medicine, Oral Pathol.*, **15**, 1259 (1962).
15. M. Giger, H. R. Baumgartner and G. Zbinden, *Agents Actions*, **4**, 173 (1974).
16. M. Israel, M. Tomasi, S. Bostel and F.-M. Meunier, *J. Neurochem.*, **78**, 658 (2001).
17. E. Zablocka-Godlewska, W. Przystas and E. Grabinska-Sota, *Water Air Soil Pollut.*, **223**, 5259 (2012).
18. V. O. Njoku, K. Y. Foo, M. Asif and B. H. Hameed, *Chem. Eng. J.*, **250**, 198 (2014).
19. S.-L. Chan, Y. P. Tan, A. H. Abdullah and S.-T. Ong, *J. Taiwan Inst. Chem. Eng.*, **61**, 306 (2016).
20. M. Ngabura, S. A. Hussain, W. A. W. Ghani, M. S. Jami and Y. P. Tan, *J. Chem. Technol. Biotechnol.*, **94**, 1384 (2019).
21. S. Lagergren, *Kungliga Svenska Vetenskapsakademiens Handlingar*, **24**, 1 (1898).
22. Y. S. Ho and G. McKay, *Process Biochem.*, **34**, 451 (1999).
23. H Yuh-Shan, *Scientometrics*, **59**, 171 (2004).
24. Y. S. Ho and G. McKay, *Process Biochem.*, **34**, 451 (1999).
25. G. Blanchard, M. Maunaye and G. Martin, *Water Res.*, **18**, 1501 (1984).
26. F. W. Cope, *Bull. Math. Biophys.*, **34**, 419 (1972).
27. H. N. Tran, S.-J. You and H.-P. Chao, *J. Environ. Chem. Eng.*, **4**, 2671 (2016).
28. H. J. Motulsky and L. A. Ransnas. *The FASEB J.*, **1**, 365 (1987).
29. Y. Gopalakrishnan, A. Al-Gheethi, M. Abdul Malek, M. Marisa Azlan, M. Al-Sahari, R. M. S. Radin Mohamed, S. Alkhadher and E. Noman, *Sustainability*, **12**, 8928 (2020).
30. B. H. Hameed and H. Hakimi, *Biochem. Eng. J.*, **39**, 338 (2008).
31. C. M. Payus, M. A. Refdin, N. Z. Zahari, A. B. Rimba, M. Geetha, C. Saroj, A. Gasparatos, K. Fukushi and P. Alvin Oliver, *Mater. Today*, **42**, 80 (2021).
32. S. J. S. Flora and V. Pachauri, *Int. J. Environ. Res. Public Health*, **7**, 2745 (2010).

33. N. F. Cardoso, E. C. Lima, I. S. Pinto, C. V. Amavisca, B. Royer, R. B. Pinto, W. S. Alencar and S. F. P. Pereira, *J. Environ. Manage.*, **92**, 1237 (2011).
34. M. A. Ahmad, N. Ahmad and O. S. Bello, *Water Air Soil Pollut.*, **225** (2014).
35. A. Witek-Krowiak, K. Chojnacka, D. Podstawczyk, A. Dawiec and K. Pokomeda, *Bioresour. Technol.*, **160**, 150 (2014).
36. K. Y. Foo and B. H. Hameed, *Chem. Eng. J.*, **187**, 53 (2012).
37. Q. Hu, S. Pang and D. Wang, *Sep. Purif. Rev.*, 1 (2021).
38. K. Y. Foo and B. H. Hameed, *Chem. Eng. J.*, **156**, 2 (2010).
39. Z. L. Yaneva and N. V. Georgieva, *Int. Rev. Chem. Eng.*, **4**, 127 (2012).
40. Y. Mihara, T. Inoue and K. Yokota, *Yakugaku Zasshi*, **125**, 225 (2005).
41. B. H. Hameed and M. I. El-Khaiary, *J. Hazard. Mater.*, **154**, 639 (2008).
42. I. Langmuir, *J. Am. Chem. Soc.*, **38**, 2221 (1916).
43. K. Y. Foo and B. H. Hameed, *Chem. Eng. J.*, **156**, 2 (2010).
44. T. W. Weber and R. K. Chakravorti, *AIChE J.*, **20**, 228 (1974).
45. K. S. Walton and R. Q. Snurr, *J. Am. Chem. Soc.*, **129**, 8552 (2007).
46. H. Freundlich, *Zeitschrift Fur Physikalische Chemie*, **57**, 385 (1906).
47. N. Sivarajasekar and R. Baskar, *Desalination Water Treat.*, **52**, 7743 (2014).
48. D. S. Jovanović, *Kolloid-Zeitschrift & Zeitschrift Fur Polymere*, **235**, 1203 (1969).
49. O. Redlich and D. L. Peterson, *J. Phys. Chem.*, **63**, 1024 (1959).
50. N. Ayawei, A. N. Ebelegi and D. Wankasi, *J. Chem.*, **2017**, e3039817 (2017).
51. Y. C. Wong, Y. S. Szeto, A. Cheung and G. Mckay, *Process Biochem.*, **39**, 695 (2004).
52. J. Toth, *Acta Chimica (Academiae Scientiarum) Hungaricae*, **69**, 311 (1971).
53. M. S. Podder and C. B. Majumder, *Water Conserv. Sci. Eng*, **1**, 21 (2016).
54. D. Do, Adsorption Analysis: Equilibria and Kinetics, Imperial College Press, London (1998).
55. Z. Saadi, R. Saadi and R. Fazaeli, *J. Nanostruct. Chem.*, **3**, 48 (2013).
56. A. B. Perez-Marin, V. M. Zapata, J. F. Ortuno, M. Aguilar, J. Saez and M. Llorens, *J. Hazard. Mater.*, **139**, 122 (2007).
57. Y. Torkia and M. Khalfaoui, *IOSR J. Appl. Phys.*, **6**, 62 (2014).
58. T. C. Chandra, M. M. Mirna, Y. Sudaryanto and S. Ismadji, *Chem. Eng. J.*, **127**, 121 (2007).
59. K. Nuithitikul, S. Srikhun and S. Hirunpraditkoon, *J. Taiwan Inst. Chem. Eng.*, **41**, 591 (2010).
60. D. Sharmmah, *AIJR Abstracts* (2021).
61. A.-A. Pelaez-Cid, A.-M. Herrera-Gonzalez, M. Salazar-Villanueva and A. Bautista-Hernandez, *J. Environ. Manage.*, **181**, 269 (2016).
62. Z. Belala, M. Jeguirim, M. Belhachemi, F. Addoun and G. Trouve, *Environ. Chem. Lett.*, **9**, 65 (2011).
63. K.-W. Jung, B. H. Choi, M.-J. Hwang, T.-U. Jeong and K.-H. Ahn, *Bioresour. Technol.*, **219**, 185 (2016).
64. H. Grabi, F. Derridj, W. Lemlikchi and E. Guenin, *Sci. Rep.*, **11**, 9705 (2021).
65. E. C. Lima, A. Hosseini-Bandegharaei, J. C. Moreno-Pirajan and I. Anastopoulos, *J. Mol. Liq.*, **273**, 425 (2019).
66. X. Zhou and X. Zhou, *Chem. Eng. Comm.*, **201**, 1459 (2014).
67. F. Kefif, K. Ezziane, A. Bahmani, N. Bettahar and S. Mayouf, *Bull. Mater. Sci.*, **42**, 14 (2019).